PROCEEDINGS A

rspa.royalsocietypublishing.org

Research

Cite this article: Erementchouk M, Joy SR, Mazumder P. 2016 Electrodynamics of spoof plasmons in periodically corrugated waveguides. *Proc. R. Soc. A* **472**: 20160616. http://dx.doi.org/10.1098/rspa.2016.0616

Received: 3 August 2016
Accepted: 21 October 2016

Subject Areas:
electromagnetism, solid state physics

Keywords:
spoof plasmons, corrugated conducting surface, terahertz plasmonics, electromagnetic waves spectrum

Author for correspondence:
Mikhail Erementchouk
e-mail: merement@umich.edu

Electrodynamics of spoof plasmons in periodically corrugated waveguides

Mikhail Erementchouk, Soumitra Roy Joy and Pinaki Mazumder

Department of Electrical Engineering and Computer Science, University of Michigan, Ann Arbor, MI 48109, USA

ME, 0000-0002-4603-1836

States of the electromagnetic field confined near a periodically corrugated surface of a perfect conductor, spoof surface plasmon polaritons (SSPP), are approached systematically based on the developed adaptation of the mode matching technique to the transfer matrix formalism. Within this approach, in the approximation of narrow grooves, systems with arbitrary transversal structure can be investigated straightforwardly, thus lifting the restrictions of the effective medium description and usual implementations of mode matching. A compact expression for the SSPP coupling parameter accounting for the effect of higher Bloch modes is found. The results of the general analysis are applied for studying the effect of dielectric environment on SSPP spectra. It is shown that the effective SSPP plasma frequency is unaffected by the dielectric constant of the medium outside of the grooves and the main effect of sufficiently wide dielectric slabs covering the corrugated surface is described by simple rescaling of the maximal value of the Bloch wavenumber and the coupling parameter. Additionally, in the case of a thin dielectric layer, it is shown that SSPP are sensitive to variation of the thickness of the layer on the sub-wavelength scale.

1. Introduction

The problem of propagation of electromagnetic waves near periodically corrugated conducting surface has attracted attention since the 1940s [1,2] in the context of slow waves and nowadays scattering of electromagnetic waves on a corrugated surface of a perfect electric conductor is one of the standard topics of textbooks

THE ROYAL SOCIETY PUBLISHING

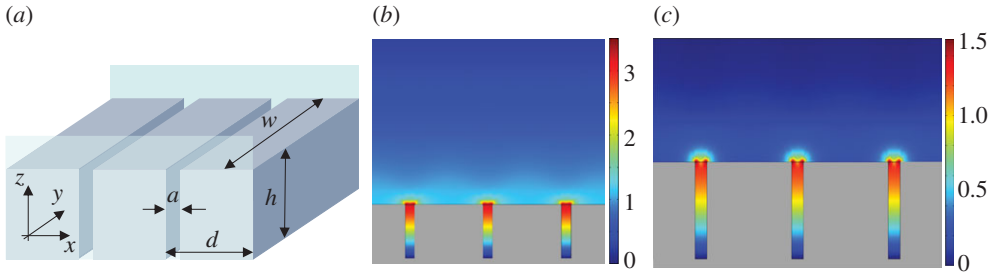

Figure 1. (*a*) A general view of the corrugated perfect conductor surface supporting spoof plasmons. Typical geometrical parameters are indicated (*a* is the width of the groove, *w* is the distance between conducting planes bounding the structure from the sides, *d* is the period of the structure, *h* is the height of the grooves) together with the choice of the coordinate system adopted in the paper. (*b*,*c*) Enhancement of the field confinement with increasing Bloch wavenumber, β: (*b*) $\beta h = 0.5\pi$, (*c*) $\beta h = 0.8\pi$. (Online version in colour.)

on electromagnetic theory. The situation has changed recently when a deep analogy between the field states and plasmons in metals has been recognized [3,4]. The grooves in the conductor, in structures similar to those shown in figure 1 play the role of cavities holding most of the field in the slow wave regime. As a result, while there is no true penetration into the material, the field is contained beneath the surface covering the structure mimicking such penetration. Moreover, as we will demonstrate below, near frequencies corresponding to the quarter-wavelength resonance of the grooves the spectrum of the electromagnetic waves can be approximately described with the help of an effective Drude model with the plasma frequency

$$\omega_{\mathrm{p}} = \frac{\pi c}{2h}. \tag{1.1}$$

Owing to such resemblance of the behaviour of true plasmon polaritons in metals, the states of the electromagnetic field confined to the corrugated surface of a perfect conductor were dubbed spoof surface plasmon polaritons (SSPP).

It should be noted, however, that the relationship between the effective plasma frequency and the parameters of the surface obtained in equation (1.1) is specific for the quasi-one-dimensional geometry, when the structure has well-defined hierarchy of sizes (along *x*-, *y*- and *z*-axes). In the two-dimensional case, where grooves have the form of cylinders, the SSPP effective plasma frequency is determined by the optical radius of the grooves [3,5] and in order to reach the regime with well-formed SSPP, it is necessary to fill grooves with a dielectric with high refractive index.

Mimicking plasmon features without penetrating into material generated a significant interest in SSPP. With the help of spoof plasmons, it becomes possible to employ various plasmon effects, for instance, field confinement and enhancement, in situations, where true plasmons can barely exist. For example, frequencies in the terahertz region are too small compared to typical metal plasma frequency and, as a result, plasmons suffer greatly from losses.

Search for adaptations of plasmon techniques to SSPP required to turn to more sophisticated structures than those, for which the SSPP effect was initially established: for example, containing layers with mismatching dielectric properties. This revealed insufficient flexibility of currently employed methods of the theoretical description of SSPP, which were successful in dealing with simple corrugated waveguides. Owing to the lack of advanced theoretical techniques, the studies of SSPP structures are restricted to numerical simulations and experimental work [6–17]. With this regard, it must be noted that even the simplest SSPP structure shown in figure 1 is characterized by four geometrical parameters resulting in a three-dimensional manifold of structures and a general theoretical guidance is needed for successful advancement.

The theoretical methods used for dealing with SSPP can be divided into two classes. One is based on the description of corrugated surfaces by an effective medium [5,18–20]. While this

approach is simple to implement technically, it suffers from two drawbacks. First, since the effective medium is homogeneous, it preserves the projection of the wavevector on the x-axis (as shown in figure 1) and thus discards the contribution of higher Bloch modes. These modes, however, play an important role when the SSPP modes are well formed and the distribution of the field outside of the grooves is highly inhomogeneous along the x-axis. Second, the parameters of the effective medium depend non-trivially on parameters of the structure, if introduction of an effective medium is possible at all [21], which makes it difficult to investigate the effect of structural variation on SSPP properties.

Another class of methods is based on the mode matching technique [22–26]. Potentially, these methods are exact but often lead to complex problems of enforcing existence of non-trivial solutions of a system of equations with respect to amplitudes of the modes. As a result, obtaining the SSPP dispersion equation in an explicit form is rather an exception [23]. To circumvent these difficulties, mode matching is often implemented under simplifying assumptions, e.g. mirror symmetry of the structure [24], significantly limiting the applicability of the method.

In this paper, we adopt the mode matching approach to the transfer matrix formulation thus introducing transversal transfer matrices. Within this approach, many problems, which are difficult to deal with using an effective medium and straightforward mode matching descriptions, are treated routinely to the point that in the approximation of narrow grooves, systems with arbitrarily complex transversal structure can be treated.

The rest of the paper is organized as follows. In §2, we introduce the general formalism of transversal transfer matrices. In §3, we discuss the general procedure of derivation of SSPP dispersion equations. In §4, spectral properties of SSPP in structures of principal importance are analysed. Finally, in §5, we apply the obtained results for studying the effect of dielectric environment on SSPP.

2. Formalism of transversal transfer matrices

The distribution of the field across a periodic structure is conveniently described within formalism of the transversal transfer matrix when the field is represented as a superposition of upward and downward propagating waves with transfer matrices relating amplitudes in different regions. The field with the polarization $E_y = 0$ can be presented inside the groove in the form

$$E_x(z < z_B) = \sum_{l=0}^{\infty} P_l \cos\left[\frac{\pi l}{a}(x - x_L)\right](f_l^{(+)}(g)\, e^{iP_l z} + f_l^{(-)}(g)\, e^{-iP_l z}), \tag{2.1}$$

where x_L is the x-coordinate of the left boundary of the groove. We will refer to the region outside of the groove as 'the arm' throughout the paper. Inside the arm, we have

$$E_x(z > z_B) = \sum_{m=-\infty}^{\infty} Q_m\, e^{i\beta_m x}\left(f_m^{(+)}(a)\, e^{iQ_m z} + f_m^{(-)}(a)\, e^{-iQ_m z}\right). \tag{2.2}$$

Here, z_B is the z-coordinate of the boundary between the groove and the arm, $f^{(\pm)}(g)$ and $f^{(\pm)}(a)$ are amplitudes inside the groove and the arm, respectively, $\beta_m = \beta + 2\pi m/d$, $Q_m^2 = P^2 - \beta_m^2$, $P_l^2 = P^2 - (\pi l/a)^2$ and $P^2 = (\omega/c)^2 - (\pi/w)^2$. In order to shorten formulae, in what follows we will omit limits of summations.

The remaining components are derived using $\nabla \cdot \mathbf{E} = 0$ and $\nabla \times \mathbf{E} = i\omega\mathbf{B}$ (here and below the time dependence is assumed in the form $e^{-i\omega t}$). Thus, inside the groove we have

$$\left.\begin{aligned} E_z(z < z_B) &= -i\sum_l \frac{\pi l}{a}\sin\left[\frac{\pi l}{a}(x - x_L)\right]\left(f_l^{(+)}(g)\, e^{iP_l z} - f_l^{(-)}(g)\, e^{-iP_l z}\right) \\ \text{and} \qquad B_y(z < z_B) &= \frac{P^2}{\omega}\sum_l \cos\left[\frac{\pi l}{a}(x - x_L)\right]\left(f_l^{(+)}(g)\, e^{iP_l z} - f_l^{(-)}(g)\, e^{-iP_l z}\right), \end{aligned}\right\} \tag{2.3}$$

and inside the arm we find

$$\left.\begin{aligned} E_z(z>z_{\mathrm{B}}) &= -\sum_m \beta_m \,\mathrm{e}^{\mathrm{i}\beta_m x}\left(f_+^{(m)}(a)\mathrm{e}^{\mathrm{i}Q_m z} - f_m^{(-)}(a)\mathrm{e}^{-\mathrm{i}Q_m z}\right) \\ \text{and}\qquad B_y(z>z_{\mathrm{B}}) &= \frac{P^2}{\omega}\sum_m \mathrm{e}^{\mathrm{i}\beta_m x}\left(f_m^{(+)}(a)\,\mathrm{e}^{\mathrm{i}Q_m z} - f_m^{(-)}(a)\,\mathrm{e}^{-\mathrm{i}Q_m z}\right). \end{aligned}\right\} \tag{2.4}$$

For a fixed z, equations (2.1) and (2.3) inside the groove and equations (2.2) and (2.4) inside the arm can be regarded as Fourier transforms of the components of the electromagnetic field as functions of x. To relate the coefficients of the expansions, we require that when z approaches the boundary between the groove and the arm from within the arm, E_x must vanish at the boundary at all x corresponding to the sides of the waveguide. Thus, incorporating the phase factors into the definition of amplitudes $f_l^{(\pm)}(g)$ and $f_m^{(\pm)}(a)$, we find

$$f_m^{(+)}(a) + f_m^{(-)}(a) = \frac{1}{Q_m d}\int_{x_{\mathrm{L}}}^{x_R} \mathrm{d}x\,\mathrm{e}^{-\mathrm{i}\beta_m x} E_x(x; z = z_{\mathrm{B}} + 0), \tag{2.5}$$

where $x_{\mathrm{R}} = x_{\mathrm{L}} + a$ is the coordinate of the right boundary of the groove, and $E_x(x; z = z_{\mathrm{B}} + 0)$ stands for E_x given by equation (2.1) taken at the boundary between the groove and the arm. The series of equations (2.5) can be rewritten in the form

$$f_m^{(+)}(a) + f_m^{(-)}(a) = \sum_l E_{m,l}(f_l^{(+)}(g) + f_l^{(-)}(g)), \tag{2.6}$$

where

$$E_{m,l} = \frac{P_l}{Q_m d}\int_{x_{\mathrm{L}}}^{x_R} \mathrm{d}x\,\mathrm{e}^{-\mathrm{i}\beta_m x}\cos\left(\frac{\pi l}{a}(x - x_{\mathrm{L}})\right). \tag{2.7}$$

The second series of equations is obtained requiring that as z approaches z_{B} from within the groove B_y must be continuous. Taking into account the relation

$$\int_{x_{\mathrm{L}}}^{x_R} \mathrm{d}x \cos\left(\frac{\pi l}{a}(x - x_{\mathrm{L}})\right)\cos\left(\frac{\pi l'}{a}(x - x_{\mathrm{L}})\right) = a s_l \delta_{l,l'}, \tag{2.8}$$

where $s_l = (1 + \delta_{l,0})/2$, we can treat expression for B_y in equation (2.3) as a Fourier series and find

$$f_l^{(+)}(g) - f_l^{(-)}(g) = \frac{1}{a s_l}\int_{x_{\mathrm{L}}}^{x_{\mathrm{R}}} \mathrm{d}x \cos\left[\frac{\pi l}{a}(x - x_{\mathrm{L}})\right] B_y(x; z = z_{\mathrm{B}} - 0) \tag{2.9}$$

or

$$f_l^{(+)}(g) - f_l^{(-)}(g) = \sum_m B_{l,m}(f_m^{(+)}(a) - f_m^{(-)}(a)), \tag{2.10}$$

where

$$B_{l,m} = \frac{1}{a s_l}\int_{x_{\mathrm{L}}}^{x_{\mathrm{R}}} \mathrm{d}x\,\mathrm{e}^{\mathrm{i}\beta_m x}\cos\left(\frac{\pi l}{a}(x - x_{\mathrm{L}})\right). \tag{2.11}$$

Equations (2.6) and (2.10) do not yet form a transfer matrix because they describe the transfer of symmetric and antisymmetric combinations of the amplitudes in opposite directions: from within the groove into the arm and from within the arm into the groove, respectively. In order to have the transfers in the same direction, equation (2.6) must be complemented by inverted equation (2.10) or another way around. This is achieved by introducing $\hat{\tilde{E}} = \hat{E}^{-1}$ and $\hat{\tilde{B}} = \hat{B}^{-1}$. Taking into account

equation (2.8) and the completeness of $\exp(\mathrm{i}\beta_m x)$ on a space of periodic functions with period d

$$\sum_m \exp(\mathrm{i}\beta_m x) = \mathrm{d}\delta(x), \tag{2.12}$$

one can check that

$$\bar{E}_{l,m} = \frac{Q_m}{P_l} B_{l,m} \quad \text{and} \quad \bar{B}_{m,l} = \frac{Q_m}{P_l} E_{m,l}. \tag{2.13}$$

Thus, equation (2.6) should be complemented by

$$f_m^{(+)}(a) - f_m^{(-)}(a) = \sum_l \bar{B}_{m,l}(f_l^{(+)}(g) - f_l^{(-)}(g)), \tag{2.14}$$

to completely express amplitudes within the arm in terms of amplitudes inside the groove and thus to fully describe transfer through the groove–arm interface. To extend this description, it is convenient to introduce a formal matrix representation of the transfer. To this end, we define vectors of states describing upward and downward propagating components

$$|f^{(\pm)}(g)) = \begin{pmatrix} f_0^{(\pm)}(g) \\ f_1^{(\pm)}(g) \\ \vdots \end{pmatrix} \quad \text{and} \quad |f^{(\pm)}(a)) = \begin{pmatrix} \vdots \\ f_{-1}^{(\pm)}(a) \\ f_0^{(\pm)}(a) \\ f_1^{(\pm)}(a) \\ \vdots \end{pmatrix}. \tag{2.15}$$

The full state of the EM field is described by the direct sum of $|f_\pm)$, which we will denote by

$$|f^{(+)}, f^{(-)}\rangle = \begin{pmatrix} |f^{(+)}) \\ |f^{(-)}) \end{pmatrix}. \tag{2.16}$$

For the field inside the groove, we denote $|\pm 1; l\rangle$ such $|f^{(+)}, f^{(-)}\rangle$, where $f_l^{(\pm)} = 1$, while the rest of the amplitudes are zero, so that an arbitrary state of the field is expanded as

$$|f^{(+)}, f^{(-)}\rangle = \sum_l f_l^{(+)} |1; l\rangle + \sum_l f_l^{(-)} |-1; l\rangle. \tag{2.17}$$

In a similar way, $|\pm 1, m\rangle$ for expanding the state vector inside the arm can be defined.

Using these notations, equations (2.6) and (2.14) can be represented in the form $|f^{(+)}(a), f^{(-)}(a)\rangle = \mathcal{T}_{\mathrm{a,g}} |f^{(+)}(g), f^{(-)}(g)\rangle$, where $\mathcal{T}_{\mathrm{a,g}} = \mathcal{T}_i(\hat{E}, \hat{\bar{B}})$ is the transfer matrix through the groove–arm interface and

$$\mathcal{T}_i(\hat{T}^{(1)}, \hat{T}^{(2)}) = \frac{1}{2} \begin{pmatrix} \hat{T}^{(1)} + \hat{T}^{(2)} & \hat{T}^{(1)} - \hat{T}^{(2)} \\ \hat{T}^{(1)} - \hat{T}^{(2)} & \hat{T}^{(1)} + \hat{T}^{(2)} \end{pmatrix} \tag{2.18}$$

is a general transfer matrix through interfaces with continuity of E_x and B_y.

The transfer matrices within the groove and the arm are found observing that while traversing them the respective amplitude simply acquire respective phase factors. Thus, for a groove with height h and for the arm with height t, we obtain

$$\mathcal{T}_{\mathrm{gg}} = \begin{pmatrix} \exp(\mathrm{i}\hat{P}h) & 0 \\ 0 & \exp(-\mathrm{i}\hat{P}h) \end{pmatrix} \tag{2.19}$$

and

$$\mathcal{T}_{\mathrm{aa}} = \begin{pmatrix} \exp(\mathrm{i}\hat{Q}t) & 0 \\ 0 & \exp(-\mathrm{i}\hat{Q}t) \end{pmatrix}, \tag{2.20}$$

respectively. Here, we have defined $\hat{P} = \mathrm{diag}(P_l)$ and $\hat{Q} = \mathrm{diag}(Q_m)$.

A case of special interest is when an element of the structure (groove or arm) contains a layer with a different dielectric function, ϵ, extending vertically over the whole element or only part of it. The expansions of the electromagnetic field in this case have the same form given by equations (2.1)–(2.4) with, respectively, modified propagation constants along the z-axis: $P^2 \to P(\epsilon)^2 = \epsilon(\omega/c)^2 - (\pi/w)^2$, $P_l^2 \to P_l^2(\epsilon) = P(\epsilon)^2 - (\pi l/a)^2$ and $Q_m^2 \to Q_m^2(\epsilon) = P^2(\epsilon) - \beta_m^2$.

The interface transfer matrix from layer characterized by $\epsilon_{\rm II}$ into the layer with $\epsilon_{\rm I}$ has the same structure within the groove and the arm

$$\mathcal{T}(\epsilon_{\rm II}, \epsilon_{\rm I}) = \mathcal{T}_i(T^{(1)}(\epsilon_{\rm II}, \epsilon_{\rm I}), T^{(2)}(\epsilon_{\rm II}, \epsilon_{\rm I})) \tag{2.21}$$

with

$$T^{(1)}_{l,l'}(\epsilon_{\rm II}, \epsilon_{\rm I}) = \frac{P_l(\epsilon_{\rm I})}{P_l(\epsilon_{\rm II})}\delta_{l,l'} \quad \text{and} \quad T^{(2)}_{l,l'}(\epsilon_{\rm II}, \epsilon_{\rm I}) = \frac{P^2(\epsilon_{\rm I})}{P^2(\epsilon_{\rm II})}\delta_{l,l'}, \tag{2.22}$$

for the groove and

$$T^{(1)}_{m,m'}(\epsilon_{\rm II}, \epsilon_{\rm I}) = \frac{Q_m(\epsilon_{\rm I})}{Q_m(\epsilon_{\rm II})}\delta_{m,m'} \quad \text{and} \quad T^{(2)}_{m,m'}(\epsilon_{\rm II}, \epsilon_{\rm I}) = \frac{P^2(\epsilon_{\rm I})}{P^2(\epsilon_{\rm II})}\delta_{m,m'}, \tag{2.23}$$

inside the arm. Finally, for the case of mismatching dielectric functions between the groove, $\epsilon_{\rm g}$, and the arm, $\epsilon_{\rm a}$ we have

$$T^{(1)}_{m,l}(\epsilon_{\rm a}, \epsilon_{\rm g}) = \frac{Q_m(\epsilon_{\rm g})}{Q_m(\epsilon_{\rm a})}E_{m,l}(\epsilon_{\rm g}) \quad \text{and} \quad T^{(2)}_{m,l}(\epsilon_{\rm a}, \epsilon_{\rm g}) = \frac{P^2(\epsilon_{\rm g})}{P^2(\epsilon_{\rm a})}\bar{B}_{m,l}(\epsilon_{\rm g}). \tag{2.24}$$

These transfer matrices can be derived by shifting infinitesimally the boundary between the regions with different refractive indices, so that it would be positioned either inside or outside the groove. Next, the transfer through the interface is performed in two steps: through the boundary between regions with different dielectric properties, which is described by either equation (2.22) or (2.23), and through the interface between arm and groove filled by the same material. It can be easily checked that the resultant transfer matrix (2.24) does not depend on the choice of the shift.

Combining the transfer matrices for individual elements, we obtain the total transfer matrix $\mathcal{T}_{\rm tot}$ connecting the state of the field at the upper and lower ends of the structure. For example, for the half-closed waveguide one has $\mathcal{T}_{\rm OS} = \mathcal{T}_{\rm ag}\mathcal{T}_{\rm gg}$.

Two features of the transfer matrices are worth emphasizing. First, the transfer matrices through either groove or arm preserve subspaces spanned by $|\pm 1; m\rangle$ and $|\pm 1; l\rangle$. To emphasize this property, we introduce more direct notations for such states defining

$$|\pm 1; \{f_l^{(\pm)}\}\rangle \equiv \sum_l f_l^{(\pm)}|\pm 1; l\rangle \tag{2.25}$$

inside the groove and analogously inside the arm. These notations provide an alternative representation of the action of transfer matrices within regions, for instance,

$$\mathcal{T}_{\rm gg}|1; \{f_l\}\rangle = |1; \{e^{iP_l h}f_l\}\rangle. \tag{2.26}$$

Second, the interface transfer matrices, as is seen directly from continuity conditions (2.6) and (2.10), establish mapping between symmetric and antisymmetric combinations of upward and downward components. To explicate this property, we define

$$|\pm x; l\rangle = \frac{1}{\sqrt{2}}(|1; l\rangle \pm |-1; l\rangle), \tag{2.27}$$

and a related version of equation (2.25)

$$|\pm x; \{g_l\}\rangle = \sum_l g_l|\pm x; l\rangle. \tag{2.28}$$

In these notations, the 'invariance' of $|\pm x\rangle$ subspaces is reflected by expressions of the form

$$\mathcal{T}_i|\pm x;\{g_l\}\rangle = |\pm x;\hat{T}^{(1,2)}\{g_l\}\rangle = |\pm x;\left\{\sum_l T^{(1,2)}_{m,l} g_l\right\}\rangle, \tag{2.29}$$

while

$$\mathcal{T}_{\mathrm{gg}}|\pm x;\{g_l\}\rangle = |\pm x;\cos(\hat{P}h)\{g_l\}\rangle + \mathrm{i}|\mp x;\sin(\hat{P}h)\{g_l\}\rangle. \tag{2.30}$$

Expressions (2.26), (2.29) and (2.30) define a representation of the transfer matrices and provide an important technical tool extensively used below.

The distribution of the field inside the structure is subject to boundary conditions determined by the form of the terminating points and by the character of the problem approached. We, first, consider the case of a groove terminated by an ideally conducting plane perpendicular to the z-axis, so that E_x must vanish at the terminating point. Thus, a state of the field at the boundary can be presented as $|\alpha\rangle = |-x;\{\alpha_l\}\rangle$ with arbitrary constants α_l. Similarly, other classes of boundary conditions can be treated. For example, waveguiding modes are characterized by radiating Sommerfeld boundary conditions at infinity. Taking for definiteness the region $z > 0$, any such state has the form $|\alpha\rangle = |1;\{\alpha_m\}\rangle$. Such defined boundary conditions together with the transfer matrices derived above deliver the complete description of the field distribution in periodic corrugated waveguides.

3. Dispersion equation for waveguiding modes

The developed formalism is directly applied for finding dispersion law governing states of the field confined to the corrugated surface, spoof surface plasmon polaritons (SSPP). The dispersion law is obtained by requiring that the transfer matrix must map state vector corresponding to the boundary condition at one point, say, $|\alpha_{\mathrm{L}}\rangle$ at the lower end, into a state vector corresponding to the condition at the opposite point, say, $|\alpha_{\mathrm{U}}\rangle$. Explicitly, this condition is written as

$$D(\omega,\beta) \equiv \langle\alpha^{\perp}_{\mathrm{U}}|\,\mathcal{T}\,|\alpha_{\mathrm{L}}\rangle = 0, \tag{3.1}$$

where $\langle\alpha^{\perp}_{\mathrm{U}}|$ is an element of space defined by $\langle\alpha^{\perp}_{\mathrm{U}}\,|\,\alpha_{\mathrm{U}}\rangle = 0$; for example, for open and closed ends, $\langle\alpha^{\perp}_{\mathrm{U}}|$ is found from $\langle x;\{\alpha^{\perp}_l\}\,|\,-x;\{\alpha_l\}\rangle = 0$ and $\langle -1;\{\alpha^{\perp}_m\}\,|\,1;\{\alpha_m\}\rangle = 0$. It should be emphasized that since for any chosen state vector $|\alpha_{\mathrm{L}}\rangle$ satisfying the boundary condition, equation (3.1) must hold for an arbitrary $\langle\alpha^{\perp}_{\mathrm{U}}|$, equation (3.1), in fact, defines a system of homogeneous equations with respect to amplitudes entering $|\alpha_{\mathrm{L}}\rangle$.

We illustrate the derivation of the dispersion law by a simple example of a slab of thickness $2t$ made of material with the dielectric function ϵ. In this case, we have only interfaces between layers with different dielectric properties and the total transfer matrix has the form $\mathcal{T} = \mathcal{T}_{\mathrm{a},\epsilon}\mathcal{T}_{\epsilon}\mathcal{T}_{\epsilon,\mathrm{a}}$, where $\mathcal{T}_{\epsilon,\mathrm{a}} = \mathcal{T}_i(\hat{T}_Q,\hat{T}_P)$ with $\hat{T}_Q$ and $\hat{T}_P$ given by $\hat{T}^{(1)}$ and $\hat{T}^{(2)}$ in equation (2.23), respectively, and $\mathcal{T}_{\epsilon} = \mathrm{diag}(\exp(2\mathrm{i}\hat{Q}(\epsilon)t),\exp(-2\mathrm{i}\hat{Q}(\epsilon)t))$. Expanding the action of the transfer matrices, we obtain $\alpha_m\beta_m D_{\mathrm{L},m} = 0$ with well known

$$D_{\mathrm{L},m} = \cos(2Q_m(\epsilon)t) - \frac{\mathrm{i}}{2}(\lambda_{\mathrm{L},m} + \lambda^{-1}_{\mathrm{L},m})\sin(2Q_m(\epsilon)t) \tag{3.2}$$

and $\lambda_{\mathrm{L},m} = T^{(2)}_m/T^{(1)}_m = Q_m(\epsilon)P^2/[Q_m P^2(\epsilon)]$, where $T^{(1,2)}_m$ are the diagonal elements of matrices $\hat{T}^{(1,2)}$ defined in equation (2.23).

Of course, for this case the formalism developed above is excessive since due to the translational symmetry the projection of the wavevector on the plane of the slab conserves and the dispersion equation can be obtained by regarding components with definite x-component of the wavevector. In the case of our main interest, when the width of the grooves is small comparing to the period of the structure, equation (3.1) can be analysed using an approximation developed similarly to the Rayleigh–Schroedinger perturbation theory. We illustrate this approach considering the SSPP dispersion equation in a half-closed waveguide (figure 4*a*), when $|\alpha_{\mathrm{L}}\rangle = |-x;\{\alpha_l\}\rangle$ and $\langle\alpha^{\perp}_{\mathrm{U}}| = \langle -1;\{\alpha^{\perp}_m\}|$. Using representation of the action of

the transfer matrix as in equations (2.29) and (2.30), we can rewrite the dispersion equation in the form

$$-\frac{1}{\sqrt{2}}\hat{\tilde{B}}\cos(\hat{P}h)|\alpha\rangle+\frac{\mathrm{i}}{\sqrt{2}}\hat{E}\sin(\hat{P}h)|\alpha\rangle=0, \tag{3.3}$$

which can be formally resolved with respect to $\cos(P_l h)\alpha_l$

$$\cos(P_l h)\alpha_l-\mathrm{i}\sum_{l'}\eta_{l,l'}\sin(P_{l'}h)\alpha_{l'}=0, \tag{3.4}$$

where $\eta_{l,l'}=(l|\hat{B}\hat{E}|l')\equiv\sum_m B_{l,m}E_{m,l'}$. Performing integration over x in $\hat{E}$ and $\hat{B}$ yields the well-known representation of the coupling parameter for $l=l'=0$ [5,22]

$$\eta_0=P_0\frac{a}{d}\sum_m\frac{1}{Q_m}\mathrm{sinc}^2\left(\frac{\beta_m a}{2}\right). \tag{3.5}$$

As this series cannot be presented in a closed form, in theoretical analysis of SSPP usually only the $m=0$ term is kept, which constitutes the single Bloch mode approximation, so that η is approximated by

$$\eta_{\mathrm{SMA}}=\frac{P_0 a}{Q_0 d}\mathrm{sinc}^2\left(\frac{\beta a}{2}\right). \tag{3.6}$$

Below we develop a more consistent approximation, which allows one to take into account the contribution of higher order Bloch modes, which play an important role in the strong confinement regime (figure 1*c*), that is when the SSPP is well formed.

Since $\eta_{l,l'}\sim a/d$, in structures with narrow grooves, equation (3.4) can be approached with the help of a perturbation theory. The most significant effect is of the first order. It yields dispersion equation of SSPP formed by modes of different orders along the x-axis inside the grooves

$$D_{\mathrm{OS},l}(\omega,\beta)\equiv\cos(P_l h)-\lambda_l\frac{P_l}{\kappa_0}\sin(P_l h)=0, \tag{3.7}$$

where we have defined $\kappa_m=\sqrt{\beta_m^2-P^2}$, and $\lambda_l\equiv\eta_{l,l}\kappa_0/P_l$ so that

$$\lambda_l=\frac{\kappa_0}{d s_l}\int_{-a}^{a}\mathrm{d}x\left[\left(1-\frac{|x|}{a}\right)\cos\left(\frac{\pi l x}{a}\right)+\frac{(-1)^l}{\pi l}\sin\left(\frac{\pi l}{a}(a-|x|)\right)\right]\mathrm{e}^{\mathrm{i}\beta x}F(x), \tag{3.8}$$

with

$$F(x)=\sum_m\frac{1}{\kappa_m}\mathrm{e}^{\mathrm{i}2\pi m x/d}. \tag{3.9}$$

While equation (3.7) describes dispersion laws of SSPPs formed by the groves modes of arbitrary order, owing to significant frequency separation between them $\sim c/a$, only the lowest one is of our interest. Therefore, we will concentrate mostly on the case $l=0$, when we have

$$\lambda_0=\kappa_0\frac{1}{d}\int_{-a}^{a}\left(1-\frac{|x|}{a}\right)\mathrm{e}^{\mathrm{i}\beta x}F(x). \tag{3.10}$$

Function $F(x)$ has logarithmic singularities at points $x=nd$ with integral n, which can be investigated by considering the vicinity of these points. Approximating the series in equation (3.9) by the main contributions, we obtain

$$F(x)\approx\frac{1}{\kappa_0}-\frac{d}{\pi}\ln\left(\frac{2\pi|x|}{d}\right). \tag{3.11}$$

The validity of this approximation in structures with narrow grooves is illustrated in figure 2. Thus, we obtain

$$\lambda_0\approx\frac{a}{d}\left\{\mathrm{sinc}^2\left(\frac{\beta a}{2}\right)+\frac{\kappa_0 d}{\pi}\left[\frac{3}{2}-\ln\left(\frac{2\pi a}{d}\right)\right]\right\}. \tag{3.12}$$

The second term in the braces, deviating from the approximation routinely used in studies of SSPP in periodically corrugated structures, η_{SMA}, accounts for the effect of multiple Bloch modes. This

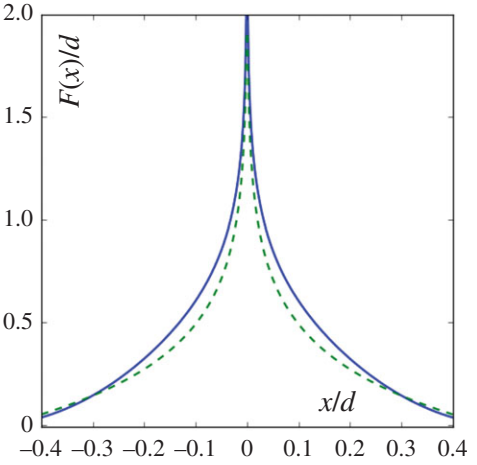

Figure 2. Function $F(x)$ (solid line) defined by equation (3.9) determining the strength of the coupling between states inside and outside the grooves and its approximation by equation (3.11) (dashed line) for β at the boundary of the Brillouin zone. (Online version in colour.)

correction, as will be shown below, becomes important in the regime of well-formed SSPP when the states of the electromagnetic field are characterized by strong confinement to the surface.

Extension of this approach to more complex structures is straightforward owing to the fact that, as long as at one end the state of the field is given by $|-x;\{\alpha_l\}\rangle$, its transfer through the structure can always be presented in the form

$$|\alpha_f\rangle = |x;\hat{T}^{(a)}\{\alpha_l\}\rangle + |-x;\hat{T}^{(b)}\{\alpha_l\}\rangle, \tag{3.13}$$

with some matrices $\hat{T}^{(a,b)}$.

The situation is different for open structures (similar to that shown in figure 4*b*), because in this case the boundary condition is set for Bloch modes of the EM field in the free space. While the same general dispersion equation, equation (3.1), holds in this case, the derivation of perturbative dispersion equation should be modified and requires finding the 'correct' representation of the state of the field inside the grooves. The general procedure goes as follows. We pick a point P inside a groove and write down the transfer matrix as a product $\mathcal{T} = \mathcal{T}_{\mathrm{U},P}\mathcal{T}_{P,\mathrm{L}}$, where $\mathcal{T}_{P,\mathrm{L}}$ is the transfer matrix from the lower end of the structure to point P and $\mathcal{T}_{\mathrm{U},P}$ propagates from point P to the upper end. The state of the field at point P is presented as $|\alpha_P\rangle = |x;\{\alpha_l^{(+)}\}\rangle - |-x;\{\alpha_l^{(-)}\}\rangle$. Propagating this state to the terminating points of the structure yields

$$\langle\alpha_{\mathrm{U}}^{\perp}|\,\mathcal{T}_{\mathrm{U},P}\,|\alpha_P\rangle = 0 \quad \text{and} \quad \langle\alpha_{\mathrm{D}}^{\perp}|\,\mathcal{T}_{P,\mathrm{L}}^{-1}\,|\alpha_P\rangle = 0, \tag{3.14}$$

which is a system of coupled equations similar to equation (3.3) and can be treated in a similar way. This strategy is used in §4b for derivation of the SSPP dispersion equation in a structure with open groove bounded from one side by a medium with mismatching dielectric function.

The situation simplifies greatly for structures with the mirror symmetry. Owing to their importance, we consider them on a slightly more general basis following the procedure sketched in [27] for the single Bloch mode approximation.

Introducing an operator switching components propagating upwards and downwards $\mathcal{S}_x = \left(\begin{smallmatrix} 0 & \hat{1} \\ \hat{1} & 0 \end{smallmatrix}\right)$, a transfer matrix through a structure possessing the mirror symmetry with respect to the plane $z = z_C$ can be factorized $\mathcal{T} = \bar{\mathcal{T}}_C\mathcal{T}_C$, where $\mathcal{T}_C$ is the transfer matrix from the lower terminating point to the symmetry plane and $\bar{\mathcal{T}}_C = \mathcal{S}_x\mathcal{T}_C\mathcal{S}_x$ is its mirror reflection. Additionally, reflection with respect to the centre must map boundary conditions at the terminating points into

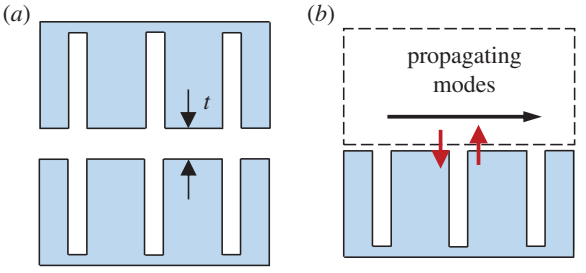

Figure 3. (*a*) The cross-section of a double-sided structure. (*b*) A schematic view of a half-closed structure in contact with a system supporting non-trivial propagating modes. (Online version in colour.)

each other leading to $|\alpha_{\mathrm{U}}\rangle = \mathcal{S}_x|\alpha_{\mathrm{L}}\rangle$. Taking into account that $[\mathcal{S}_x, \mathcal{T}_i] = 0$ and $\mathcal{S}_x\mathcal{T}_{\mathrm{aa,gg}}\mathcal{S}_x = \mathcal{T}^{-1}_{\mathrm{aa,gg}}$ we find that equation (3.1) holds when $D^{(\mathrm{e})}(\omega, \beta) = 0$ or $D^{(\mathrm{o})}(\omega, \beta) = 0$, where

$$D^{(\mathrm{e,o})}(\omega, \beta) = \langle \pm x|\, \mathcal{T}_C\, |\alpha_{\mathrm{L}}\rangle. \tag{3.15}$$

It should be noted that the definition of even and odd modes in this case is somewhat arbitrary. Here, we adopt the same convention as used in previous publications [24,27] and assign the symmetry according to the parity of E_z: even mode corresponds to the even function $E_z(z - z_C)$ and so on. Applying these results, for instance, for a dielectric slab, yields the factorization $D_{\mathrm{L}}(\omega, \beta) = D^{(\mathrm{e})}_{\mathrm{L}}(\omega, \beta)D^{(\mathrm{o})}_{\mathrm{L}}(\omega, \beta)$ with

$$D^{(\mathrm{e,o})}_{\mathrm{L},m}(\omega, \beta) = \cos(Q_m(\epsilon)t) - \mathrm{i}\lambda^{\mp 1}_{\mathrm{L},m} \sin(Q_m(\epsilon)t). \tag{3.16}$$

In the open groove waveguide, $D^{(\mathrm{e})}(\omega, \beta) = 0$, determining the dispersion law of the even SSPP mode, produces the same dispersion equation as equation (3.4) with substituted $h \to h/2$ as it should be, because these modes correspond to vanishing E_x at the middle of the groove thus effectively splitting the structure into two half-closed waveguides. In turn, $D^{(\mathrm{o})}(\omega, \beta) = 0$ yields the dispersion equation for odd modes, which for $l = 0$ has the form

$$D^{(\mathrm{o})}_{\mathrm{open}}(\omega, \beta) = \sin\left(\frac{Ph}{2}\right) + \lambda_0 \frac{P}{\kappa_0} \cos\left(\frac{Ph}{2}\right). \tag{3.17}$$

As a more involved application of the symmetry approach, we derive the dispersion equation of double-sided corrugated waveguide shown in figure 3*a*. The total transfer matrix through such structure has the form $\mathcal{T} = \mathcal{T}_{\mathrm{gg}}\mathcal{T}_{\mathrm{ga}}\mathcal{T}_{\mathrm{aa}}\mathcal{T}_{\mathrm{ag}}\mathcal{T}_{\mathrm{gg}}$ and, thus, can be factorized with $\mathcal{T}_C = \mathcal{T}^{1/2}_{\mathrm{aa}}\mathcal{T}_{\mathrm{gg}}$. The dispersion equations for the even and odd modes are given by equation (3.15) and for $l = 0$ and have the same structure as for a half-closed waveguide (see equation (3.7))

$$D^{(\mathrm{e,o})}(\omega, \beta) = \cos(Ph) - \lambda_{\mathrm{e,o}} \frac{P}{\kappa_0} \sin(Ph), \tag{3.18}$$

where

$$\lambda_{\mathrm{e,o}} = \pm \frac{\kappa_0}{P_0} \sum_m B_{0,m} \tan^{\mp 1}(Q_m t) E_{m,0}. \tag{3.19}$$

Assuming that the arm is not too narrow, $t > d/2\pi$, so that the coupling between the sides of the structure mediated by the higher order Bloch modes can be regarded as weak, we can use the same approach as for derivation of equation (3.12) and obtain

$$\lambda_{\mathrm{e,o}} = \frac{a}{d}\left\{\mathrm{sinc}^2\left(\frac{\beta a}{2}\right)\tanh^{\mp 1}(\kappa_0 t) + \frac{\kappa_0 d}{\pi}\left[\frac{3}{2} - \ln\left(\frac{2\pi a}{d}\right)\right]\right\}. \tag{3.20}$$

The appearance of the dispersion equation for a half-closed structure signifying the emergence of SSPP is not accidental. On the one hand, taking the projection on $l = 0$ states reduces the transversal distribution of the field in the structure to renormalization of parameters

characterizing $l=0$ SSPP mode. On the other hand, the field distribution can be presented as a result of coupling SSPP with waveguiding modes in the rest of the structure. In order to explicate this statement, we consider a structure schematically shown in figure 3*b*, where the closed groves with the interface at $z=z_B$ serve as a terminating point. The transfer matrix through such structure factorizes $\mathcal{T}=\mathcal{T}_{U,B}\mathcal{T}_{OS}$, where $\mathcal{T}_{U,B}$ is the transfer matrix from the interface with the half-closed structure to the opposite terminating point. Assuming that the boundary condition at that point is described by vectors $|\alpha\rangle$, the dispersion equation of the states in the complex structure is $D(\omega,\beta)=\langle\alpha^{\perp}|\,\mathcal{T}_{U,B}\mathcal{T}_{OS}\,|-x\rangle$. Introducing a formal resolution of identity

$$\mathcal{I}=\sum_{\gamma}(|1,\gamma\rangle\langle 1,\gamma|+|-1,\gamma\rangle\langle -1,\gamma|), \tag{3.21}$$

with the summation running over an appropriate set of γ, we obtain

$$D(\omega,\beta)=D_{U,B}(\omega,\beta)D_{OS}(\omega,\beta)-\Lambda, \tag{3.22}$$

where $D_{OS}=\langle -1|\,\mathcal{T}_{OS}\,|-x\rangle$ describes SSPP in the half-closed structure, $D_{U,B}=\langle\alpha^{\perp}|\,\mathcal{T}_{U,B}\,|-1\rangle$ defines the dispersion equation of waveguiding modes in the rest of the structure and

$$\Lambda=\langle\alpha^{\perp}|\,\mathcal{T}_{U,B}\,|1\rangle\langle 1|\,\mathcal{T}_{OS}\,|-x\rangle \tag{3.23}$$

describes coupling between SSPP and waveguiding modes.

In §4c, we will apply this consideration for an analysis of some general features of double-sided structures.

4. Dispersion law of spoof surface plasmon polaritons

In this section, we analyse in details the dispersion law of SSPP in structures of main interest and find the relationship between spectral characteristics and geometry and dielectric properties of the structure.

(a) Half-closed waveguide

The simplest SSPP structure is a one-sided waveguide, which is essentially just a conducting corrugated surface (figure 4*a*). The SSPP dispersion law for such structure is determined by equation (3.7), which for the lowest frequency SSPPs (with $l=0$) has the form

$$\cos(Ph)-\lambda\frac{P}{\kappa}\sin(Ph). \tag{4.1}$$

Here η is given by equation (3.12) and, as we are interested only in the $l=0$ mode, we omit index 0.

Equation (4.1) was a subject of numerous investigations and the main features of the SSPP spectrum are well studied. Owing to the importance of this equation, however, we review its solutions here and will often refer to this analysis throughout the rest of the paper.

First, we would like to clarify the analogy with true plasmons outlined in the Introduction. To this end, we compare equation (4.1) with the dispersion equation for the true surface plasmon polaritons at the interface between air and metal with dielectric constant ϵ_m

$$\sqrt{\frac{\beta^2-(\omega/c)^2}{\beta^2-\epsilon_m(\omega/c)^2}}=-\frac{1}{\epsilon_m}. \tag{4.2}$$

Defining ϵ_m in such way that both equations (4.1) and (4.2) represent the same equation and excluding β with the help of equation (4.1), we find

$$\epsilon_m=\frac{1}{\lambda^2}\left(1-\lambda-\frac{1}{\sin^2(\omega h/c)}\right)\sim\frac{1}{\lambda^2}\left(1-\frac{\omega_p^2}{\omega^2}\right), \tag{4.3}$$

where $\omega_p=\pi c/2h$ is the effective plasma frequency for the SSPP defined by the condition of vanishing effective dielectric function $\epsilon_m(\omega=\omega_p)=0$. This shows that, indeed, from the spectral

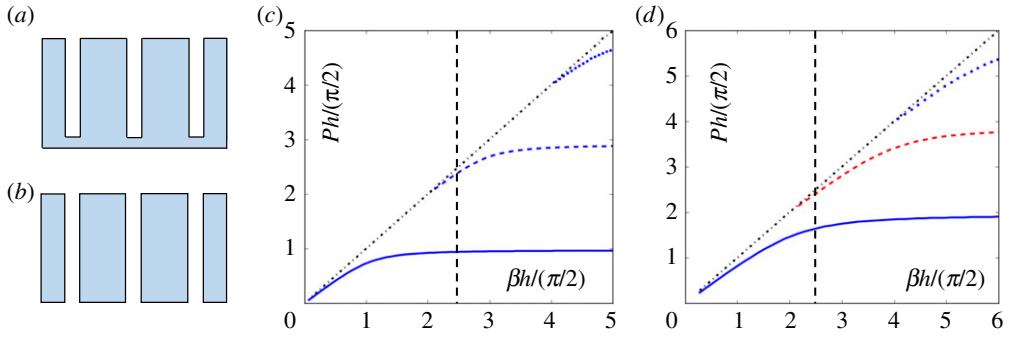

Figure 4. Half-closed and open SSPP structures. (*a*,*b*) The cross-sections of half-closed and open waveguides, respectively. (*c*,*d*) Dispersion diagrams on the (Ph, βh)-plane of SSPP in half-closed and open waveguides, respectively. The vertical and horizontal axes are additionally rescaled by $\pi/2$, so that the coordinates of the characteristic points are expressed in integer numbers. The dash-dotted line shows the light line, $\omega = \beta c$. The vertical dashed line shows the right boundary of the dispersion diagrams determined by $\beta_{\max} = \pi/d$ in a structure with $h/d = 5$. (Online version in colour.)

point of view, the electromagnetic waves confined near the corrugated surface look similar to surface plasmon polaritons.

In order to outline the main effect of the geometry of the structure, we note that spectral and geometrical parameters enter equation (4.1) through three variables: Ph, βh and η. Therefore, SSPP dispersion diagrams of all half-closed structures have the same overall form shown in figure 4*c*. In wide structures, where $\pi c/w \ll \omega_{\mathrm{p}}$, the transition from weakly attenuated to SSPP regime occurs near $\beta = \beta_c = \omega_{\mathrm{p}}/c$, where the light-line intersects the effective plasma frequency. Below the transition, $\beta < \beta_c$, the dispersion curve only slightly deviates from the light-line, and for $\beta > \beta_c$ the dispersion curve gradually approaches ω_{p}. Thus, varying the geometry of the structure will only change the 'smoothness' of transition between two regimes on the (Ph, βh)-plane and, if the period is changed, will limit the dispersion diagram at different $(\beta h)_{\max} = \pi h/d$.

The form of the dispersion curve is determined by a set of characteristic frequencies. First, these are frequencies ω_P and $\omega_\kappa(\beta)$ at which $P(\omega)$ and $\kappa(\omega, \beta)$ vanish. The curve $\omega = \omega_\kappa(\beta)$ separates regions corresponding to propagating and attenuated modes outside of the grooves and thus defines the light-line. For example, in the case $w \to \infty$, we have $\omega_P = 0$ and $\omega_\kappa(\beta) = \beta c$. Another set of characteristic frequencies, $\omega_{\mathrm{p}}^{(n)}$, is given by the positions of zeros of $\cos(Ph)$, so that $P(\omega = \omega_{\mathrm{p}}^{(n)}) = \pi(1/2 + n)/h$ with integer n.

From the relationships between the characteristic frequencies, it can be seen that for all β's, equation (4.1) has at least one solution, which we will call the fundamental branch. Its character strongly depends on the relationship between $\omega_Q(\beta)$ and $\omega_{\mathrm{p}}^{(n)}$, that is between the light-line and SSPP plasma frequencies. Indeed, in the case of small β, when $\omega_Q(\beta) \ll \omega_{\mathrm{p}}^{(n)}$, we find

$$P^2 \approx \beta^2(1 - \lambda^2\beta^2h^2). \tag{4.4}$$

Taking into account the relation $\omega^2 = (\pi c/w)^2 + P^2c^2$, such represented solution is valid for arbitrary width of the structure and the dielectric function of the medium. This solution only slightly deviates from the light line and thus corresponds to weakly attenuated field outside of the grooves.

In the opposite limit, $\omega_Q(\beta) \gg \omega_{\mathrm{p}}^{(0)}$, the solution is close to $\omega_{\mathrm{p}}^{(0)}$, so that

$$P \approx \frac{\pi}{2h} - \frac{\pi\lambda}{2\beta h^2}. \tag{4.5}$$

Thus, we have significant deviation from the light line, which corresponds to strong attenuation of the field outside of the grooves. The transition between regimes of weak and strong confinement occurs near the crossing of the light-line and the SSPP plasma frequency, i.e. $\omega_Q(\beta_c) = \omega_{\mathrm{p}}^{(0)}$.

This consideration suggests to identify the strong confinement regime with the formation of SSPP, because it corresponds to emergence of the effective Drude model as expressed by the second half of equation (4.3). As β is limited by the Brillouin zone, $\beta \leq \beta_{\max} = \pi/d$, this yields the criterion that the corrugated surface must satisfy in order to support well-defined SSPP, $\beta_c < \pi/d$ or

$$h > \frac{d}{2}. \tag{4.6}$$

Thus, the effect of SSPP can be expected to be well developed in structures with sufficiently long grooves. With increasing length of the groove, the characteristic frequencies $\omega_{\mathrm{p}}^{(n)}$ decrease, which may lead to the appearance of additional bands. It can be seen that the number of branches at given β equals to $1 + n_{\max}$, where $n_{\max}$ is maximal n such that $\omega_P^{(n)} < \omega_Q(\beta)$ with $\omega_P^{(n)}$ defined as zeros $\sin(Ph)$ in equation (4.1), so that $P(\omega = \omega_P^{(n)}) = \pi n$. The analysis of the nth higher branch can be performed using the same arguments as above with substitutions $\omega_P \to \omega_P^{(n)}$ and $\omega_{\mathrm{p}}^{(0)} \to \omega_{\mathrm{p}}^{(n)}$. Without going into such detailed analysis, we limit ourselves to noticing an interesting feature of the higher branches. In contrast to the fundamental branch, they exist only when β is large enough (figure 4) $\beta > \beta_0^{(n)}$, where $\beta_0^{(n)}$ is found from $\omega_Q(\beta_0^{(n)}) = \omega_P^{(n)}$, which yields the condition for the nth-order band to exist. For example, in wide waveguides with $w > h$, the nth higher band appears when $h > nd$.

The important characteristics of the SSPP, the position of the edge of the fundamental band, is found from equation (4.5) by taking $\beta = \beta_{\max}$. In wide structures, where the effect of the cut-off frequency $\pi c/w$ can be neglected, with sufficiently long grooves, $h > d/2$, one has

$$\omega_{\mathrm{e}} = \omega_{\mathrm{p}} - \Delta\omega_{\mathrm{e}}, \tag{4.7}$$

where the frequency separation between the edge of the fundamental band and the plasma frequency in the approximation of narrow grooves is found to be

$$\Delta\omega_{\mathrm{e}} \approx \frac{2\lambda_{\mathrm{B}}\omega_{\mathrm{p}}}{\pi\sqrt{(2h/d)^2 - 1}}, \tag{4.8}$$

with $\lambda_{\mathrm{B}} = \lambda(\omega = \omega_{\mathrm{p}}, \beta = \beta_{\max})$. Respectively, the gap separating the fundamental band from the next band in structures with $h > d$ has the width

$$\Delta_0 = \omega_{\mathrm{p}}(1 + \delta_0). \tag{4.9}$$

The dependence of the position of the edge of the fundamental band on the groove height predicted by this expression is in excellent agreement with the results of full-wave numerical simulations in finite-element software [28] as is shown in figure 6*b*.

(b) Open structure

As we have seen above, in structures with open grooves, there are two classes of SSPP modes corresponding to different transformation properties under reflection about the (x, y)-plane passing through the centre of the grooves. Even modes are characterized by vanishing E_x at $z = z_C$ and, as a result, the dispersion equation of even modes reproduces that of half-closed structures with renormalized grooves height $h \to h/2$ as is illustrated by figure 5*a*. Thus, the consideration provided above directly applies to even modes in structures with open grooves.

The spectrum of odd modes is determined by equation (3.17), which is convenient to study by introducing the phase parameter $\xi = Ph - \pi/2$ or $\tilde{P} = P - \pi/2h$. Equation relating $\tilde{P}$ and β has the structure similar to equation (4.1) and can be analysed in a similar manner by considering relationships between characteristic frequencies.

It follows from this analysis that odd modes are similar to higher order bands: they appear in structures with sufficiently long grooves, $h > d$, start from non-zero $\beta_o^{(n)} = \pi(1 + 2n)/h$ and occupy bands approaching effective plasma frequencies $\omega_o^{(n)} = (1 + n)2\pi c/h$ and situated between the bands of even modes.

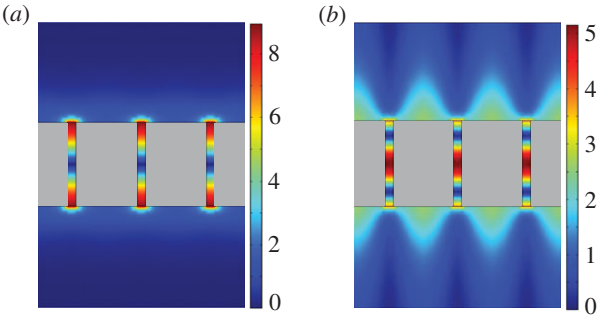

Figure 5. Electromagnetic field energy distribution in structures with open grooves with $h/d = 1.6$ at $\beta = \beta_{\max}$. (*a*) Even modes with $E_x = 0$ at the line passing through the centre of the grooves are analogous to states in half-closed waveguides with the grooves of halved height. (*b*) Odd modes bands reside in the gaps left by the even modes. Their distinctive feature is the symmetry of the field distribution. The difference between panels (*a*) and (*b*) is due to reduced attenuation and increased contrast of beatings in higher bands comparing to the fundamental band. Far, comparing to *a*, away from the opening of the grooves, the main contribution is due to the $m = 0$ and $m = -1$ components leading to formation of a universal pattern $W \sim \mathrm{e}^{-2\kappa z}(1 - (P/\beta)^2 \cos^2(\pi x/d))$, where x is counted from the centre of a groove. Thus, increasing the band number results in a more prominent 'far zone' distribution due to reduced κ and increased P/β. (Online version in colour.)

The general structure of the spectrum of structures with open grooves is shown in figure 4*d*. While it looks similar to the spectrum of half-closed structure, an important difference should be noted. Odd branches occupy the space between even branches, which leads to a significant reduction of the band gaps. Starting point of odd bands is the spoof plasma frequency of the previous even band. As a result, the band gaps are determined solely by the distance between the edges of the bands and the respective plasma frequencies.

(c) Double-sided structure

SSPP in double-sided structures (figure 3*a*) enjoyed significant attention [8,24,29]. Because of this and in view of the similarity of the dispersion equations governing modes of double-sided corrugated waveguides (equations (3.18)) and half-closed structures (equation (4.1)), so that the same analysis can be performed, we limit ourselves to discussion of some general properties only.

As the structure is closed, solutions of the dispersion equation must be sought for in a class of non-attenuated states outside of the grooves (i.e. with real Q) as well. In order to outline the consequences of this circumstance, we apply the consideration illustrated at the end of §3.

Let the transfer matrices through the lower and the upper groove be $\mathcal{T}_{\mathrm{OS}}^{(1,2)}$, respectively, and the transfer across the arm is described by $\mathcal{T}_a$. Then, the dispersion equation can be presented schematically as

$$D(\omega, \beta) = D_{\mathrm{OS}}^{(1)} \langle -1 | \, \mathcal{T}_{\mathrm{a}} \, | -1 \rangle D_{\mathrm{OS}}^{(2)} - \Lambda(\omega, \beta), \tag{4.10}$$

where $D_{\mathrm{OS}}^{(1)} = \langle x | \, \mathcal{T}_{\mathrm{OS}}^{(2)} \, | -1 \rangle$ can be seen to yield the dispersion equation for the second half-closed waveguide, $D_{\mathrm{OS}}^{(2)} = \langle -1 | \, \mathcal{T}_{\mathrm{OS}}^{(1)} \, | -x \rangle$, and $\Lambda(\omega, \beta) = \langle x | \, \mathcal{T}_{\mathrm{OS}}^{(2)} \, | 1 \rangle \langle 1 | \, \mathcal{T}_{\mathrm{a}} \, | 1 \rangle \langle 1 | \, \mathcal{T}_{\mathrm{OS}}^{(1)} \, | -x \rangle$. Expressions for $D(\omega, \beta)$ and $\Lambda(\omega, \beta)$ contain diagonal elements of the transfer matrix through the arm. Depending on whether the states inside the arm are attenuated or not (i.e. $\beta > \beta_c$ or $\beta \sim 0$), the effect of the coupling between opposite sides of the waveguide is drastically different.

When $\beta > \beta_c$, the coupling parameter is exponentially small, $\sim \mathrm{e}^{-2\kappa_0 t}$. As a result, in this region we have weakly coupled modes at the opposite sides of the waveguide. In symmetric structure, this leads to slightly repelled symmetric and antisymmetric modes. Using equation (3.20) in the expression for the band edge (equation (4.7)), we find exponentially decreasing with the arm

width the separation between the edges of even and odd modes

$$\Delta = \omega_{\mathrm{p}} \frac{a}{h} \frac{\mathrm{sinc}^2(\beta a/2)}{\sinh(2\kappa t)}, \tag{4.11}$$

where $\kappa t = \pi t d^{-1}\sqrt{1-(d/2h)^2}$.

In the opposite case, $\beta \sim 0$, the matrix elements of $\mathcal{T}_a$ are pure phase factors and, as a result, we have strong coupling of modes confined to opposite sides. As a result, at $\beta = 0$, the even branch resides at $P \approx 0$, while the odd branch is at $P = \pi/2h(1-\delta)$ with

$$\delta \approx \frac{a}{d}\left\{\tan\left(\frac{\pi t}{2h}\right) + \frac{d}{2h}\left[\frac{3}{2} - \ln\left(\frac{2\pi a}{d}\right)\right]\right\}. \tag{4.12}$$

Moreover, one can see that if the arm is not too wide, for small β one has $\tanh(\kappa t) \approx \kappa t$, which cancels κ from the dispersion equation making the even branch dispersionless.

5. The effect of the dielectric environment

Consideration of states of the field in corrugated structures from the plasmon perspective naturally raises an interest in the interaction with matter. As the first step in this direction, this requires analysis of the effect of media surrounding the conductor on SSPP spectral properties. The simplest situation is when the space outside of the conductor is filled with material with the dielectric function ϵ. This can be accounted for by simple rescaling frequency $\omega \to \omega/\sqrt{\epsilon}$ and not only the results formulated above in terms of P stay the same but the dispersion diagrams on the $(Ph, \beta h)$-plane (figure 4) remain unchanged.

When the structure contains interfaces between regions with mismatched dielectric properties, however, the variation of the SSPP spectrum is more complex. Some of such situations do not succumb to currently used analytical methods and require resorting to numerical simulations. In this section, we will demonstrate, how the transfer matrix approach can be used for analysis of SSPP spectra in these cases.

(a) Half-closed waveguide covered by an infinite dielectric slab

We start by considering the case when the interior of the grooves of a half-closed waveguide and the outside space are filled with materials with different dielectric constants, ϵ_{g} and ϵ_{a}, respectively (figure 6*a*). The mismatch between ϵ_{g} and ϵ_{a} leads to modification of the interface transfer matrix $\mathcal{T}_{\mathrm{ag}}$ according to equations (2.24). It can be seen that in this case the SSPP dispersion equation has the same general form as for a dielectrically homogeneous environment

$$\cos(Ph) - \lambda(\epsilon_{\mathrm{a}})\frac{P^2(\epsilon_{\mathrm{a}})}{P^2(\epsilon_{\mathrm{g}})}\frac{P(\epsilon_{\mathrm{g}})}{\kappa(\epsilon_{\mathrm{a}})}\sin(Ph) = 0, \tag{5.1}$$

where $\kappa(\epsilon_{\mathrm{a}}) = \sqrt{\beta^2 - P^2(\epsilon_{\mathrm{a}})}$ and $\lambda(\epsilon_{\mathrm{a}})$ is given by equation (3.12) with κ replaced by $\kappa(\epsilon_{\mathrm{a}})$.

Changes induced by the dielectric environment in this case are quite straightforward. We discuss them in the limit $w \to \infty$, when after introducing $\tilde{P} = \sqrt{\epsilon_{\mathrm{a}}}\omega/c$ and $\tilde{h} = h\sqrt{\epsilon_{\mathrm{g}}/\epsilon_{\mathrm{a}}}$ we arrive at the same equation as equation (4.1) with rescaled coupling parameter $\lambda \to \lambda\sqrt{\epsilon_{\mathrm{a}}/\epsilon_{\mathrm{g}}}$. Thus, in the $(\tilde{P}(\epsilon_{\mathrm{a}})\tilde{h}, \beta\tilde{h})$-plane, the only variation in the SSPP spectrum is in the crossover from low attenuated to the SSPP regime due to renormalized λ, as is demonstrated in figure 6*b*. In particular, the SSPP plasma frequency is defined by the same condition $\tilde{P}\tilde{h} = \pi/2$ leading to $\tilde{\omega}_{\mathrm{p}} = \omega_{\mathrm{p}}/\sqrt{\epsilon_{\mathrm{g}}}$.

The results obtained above for the half-closed waveguide can be directly applied for this case. In particular, the position of the edge of the fundamental band can be found from equations (4.7) and (4.8): $\omega_{\mathrm{e}} = \tilde{\omega}_{\mathrm{p}} - \Delta\omega_{\mathrm{e}}(\epsilon_{\mathrm{a}}, \epsilon_{\mathrm{g}})$, where

$$\Delta\omega_{\mathrm{e}}(\epsilon_{\mathrm{a}}, \epsilon_{\mathrm{g}}) = \tilde{\omega}_{\mathrm{p}}\sqrt{\frac{\epsilon_{\mathrm{a}}}{\epsilon_{\mathrm{g}}}}\frac{2\lambda(\epsilon_{\mathrm{a}})}{\pi\sqrt{(2h/d)^2\epsilon_{\mathrm{g}}/\epsilon_{\mathrm{a}} - 1}}. \tag{5.2}$$

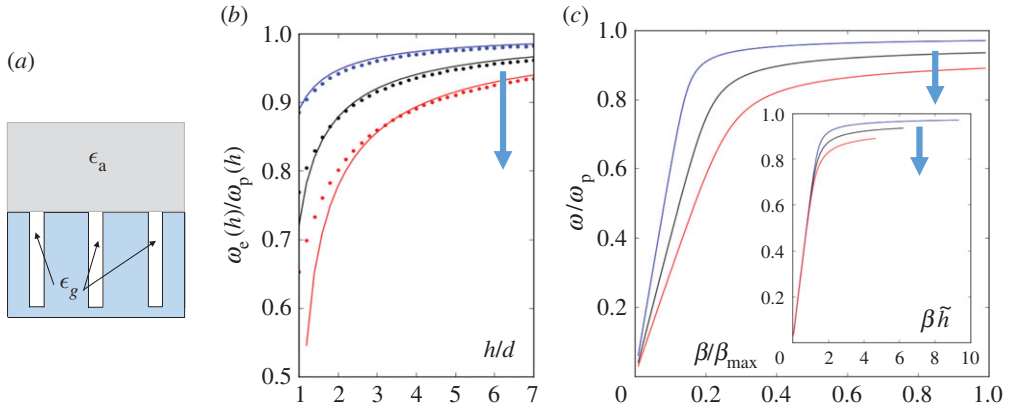

Figure 6. (*a*) The cross section of a half-closed waveguide filled by material with the dielectric function ϵ_g bounded by half-space with the dielectric function ϵ_a. (*b*) The normalized position of the edge of the fundamental band $\omega_e(h)/\tilde{\omega}_p(h)$ as a function of the grooves height for different values of ϵ_a (the arrows show the variation with increasing $\epsilon_a = 1, 2.25, 4$): solid lines are obtained from equation (5.2), dotted lines show the results of full-wave numerical simulations. (*c*) Variation of the SSPP dispersion diagram with the refractive index of the surrounding medium. The inset shows the dispersion diagrams in rescaled parametrization $\omega(\beta\tilde{h})$. (Online version in colour.)

Its dependence on the height of the groove is shown in figure 6*b* together with the results of full-wave numerical simulations. It demonstrates, in particular, that as long as the system is in the SSPP regime, $\beta\tilde{h} > \pi/2$, equation (5.2) agrees very well with numerical simulations.

We conclude consideration of this case emphasizing two circumstances. First, the spoof plasma frequency is determined solely by the optical height of the grooves $h\sqrt{\epsilon_g}$ and dielectric properties of the arm leave it unaffected. This is due to the strong attenuation of the electromagnetic field outside of the grooves in the limit $\beta h \gg 1$. As a result, the effect of the dielectric properties of surrounding medium becomes negligible. Second, in the case $\epsilon_g = 1$, the main variation of the SSPP spectrum is accounted for by effective renormalization $h \to h/\sqrt{\epsilon_a}$. This leads to decreasing value of the cut-off point $\beta_{max}\tilde{h}$ on the dispersion diagram as is evident from figure 6*c*. This reduction of the SSPP regime is due to reduced confinement inside the dielectric.

(b) Open waveguide covered by a semi-infinite dielectric slab

A structure with open grooves in contact on one side with a medium with the dielectric function ϵ presents a special interest from the perspective of adopting plasmon techniques for SSPP. In this particular case, SSPP can be excited from one side using, say, Otto prism [30,31], while interacting with a tested material on the other side. Such structures are difficult to deal with using standard approaches because of, on the one hand, the lack of mirror symmetry and, on the other hand, the necessity to match two infinite sets of amplitudes characterizing Bloch modes in half-spaces separated by the SSPP waveguide. This obstacle is avoided in the transfer matrix formalism and we use this situation for showing in details calculations within the developed formalism.

Having in mind establishing a relation with the symmetric case, we choose the state at the centre of the groove in the form

$$|\alpha\rangle = |x, \{\alpha_l^{(+)}\}\rangle + |-x, \{\alpha_l^{(-)}\}\rangle. \tag{5.3}$$

State $|\alpha\rangle$ must be mapped by the transfer matrices through the halves of the structure into correct boundary conditions. Thus for two arbitrary sets of amplitudes $\{\gamma_m^{(u,d)}\}$, we must have

$$\langle -1, \{\gamma_m^{(u)}\}| \mathcal{T}_{ag}\mathcal{T}_g^{1/2} |\alpha\rangle = 0 \quad \text{and} \quad \langle 1, \{\gamma_m^{(d)}\}| \mathcal{T}_{lg}\mathcal{T}_g^{-1/2} |\alpha\rangle = 0, \tag{5.4}$$

where we denote $\mathcal{T}_{ag}=\mathcal{T}_i(\hat{T}_U^{(1)},\hat{T}_U^{(2)})$ and $\mathcal{T}_{lg}=\mathcal{T}_i(\hat{T}_D^{(1)},\hat{T}_D^{(2)})$ with $\hat{T}_U^{(1)}=\hat{E}$, $\hat{T}_U^{(2)}=\hat{\tilde{B}}$ and $\hat{T}_D^{(1,2)}$ given by equation (2.24). Expanding equations (5.4) we obtain

$$\left.\begin{aligned}&(\gamma^{(u)}|[\hat{T}_U^{(1)}\cos(\hat{P}h/2)-\mathrm{i}\hat{T}_U^{(2)}\sin(\hat{P}h/2)]|\alpha^{(+)})\\&\quad-(\gamma^{(u)}|[\hat{T}_U^{(2)}\cos(\hat{P}h/2)-\mathrm{i}\hat{T}_U^{(1)}\sin(\hat{P}h/2)]|\alpha^{(-)})=0\\\text{and}\quad&\left(\gamma^{(d)}\left|\left[\hat{T}_D^{(1)}\cos\left(\frac{\hat{P}h}{2}\right)-\mathrm{i}\hat{T}_D^{(2)}\sin\left(\frac{\hat{P}h}{2}\right)\right]\right|\alpha^{(+)}\right)\\&\quad+\left(\gamma^{(d)}\left|\left[\hat{T}_D^{(2)}\cos\left(\frac{\hat{P}h}{2}\right)-\mathrm{i}\hat{T}_D^{(1)}\sin\left(\frac{\hat{P}h}{2}\right)\right]\right|\alpha^{(-)}\right)=0.\end{aligned}\right\}\tag{5.5}$$

Now, we take into account that these are combinations of the form $\hat{\tilde{T}}^{(2)}\hat{T}^{(1)}$ that provide a small parameter in the perturbation theory (cf. with equations (3.3) and (3.4)) and represent

$$(\gamma^{(u,d)}|=(\tilde{\gamma}^{(u,d)}|\hat{T}_{U,D}^{(2)},\tag{5.6}$$

where amplitudes $\tilde{\beta}$ define a state in the space of groove modes. Using this representation in equation (5.5) and taking the first order of the perturbation theory, we obtain for $l=0$

$$\left.\begin{aligned}&\left[\eta_U\cos\left(\frac{Ph}{2}\right)-\mathrm{i}\sin\left(\frac{Ph}{2}\right)\right]\alpha_0^{(+)}-\left[\cos\left(\frac{Ph}{2}\right)-\mathrm{i}\eta_U\sin\left(\frac{Ph}{2}\right)\right]^{\alpha_0^{(-)}=0}\\\text{and}\quad&\left[\eta_D\cos\left(\frac{Ph}{2}\right)-\mathrm{i}\sin\left(\frac{Ph}{2}\right)\right]\alpha_0^{(+)}-\left[\cos\left(\frac{Ph}{2}\right)-\mathrm{i}\eta_D\sin\left(\frac{Ph}{2}\right)\right]^{\alpha_0^{(-)}=0,}\end{aligned}\right\}\tag{5.7}$$

where $\eta_{U,D}=(l=0|\hat{\tilde{T}}_{U,D}^{(2)}\hat{T}_{U,D}^{(1)}|l=0)$ and, thus, have the same form as for the half-closed waveguide surrounded by air (for η_U) and by a semi-infinite dielectric slab (for η_D). Requiring that equations (5.7) have a non-trivial solution, we find the dispersion equation in the form

$$D_{\mathrm{open}}^{(e)}(\omega,\beta)D_{\mathrm{open}}^{(o)}(\omega,\beta)-\Delta\eta^2\sin\left(\frac{Ph}{2}\right)\cos\left(\frac{Ph}{2}\right)=0,\tag{5.8}$$

where $\Delta\eta=(\eta_U-\eta_D)/2$ and $D_{\mathrm{open}}^{(e,o)}(\omega,\beta)$ are given by the dispersion equations of even and odd modes of a structure with open grooves with the coupling parameter $\eta=(\eta_U+\eta_D)/2$.

Equation (5.8) demonstrates that when the mirror symmetry is broken, the modes of the open structure are coupled. The effect of the coupling, however, is the strongest at the crossover region. For example, in the SSPP regime $\cos(Ph/2)\approx\Delta\omega_e/\omega_p$ which leads to corrections of the next order in a/d. Thus, due to the separation between even and odd bands, $D_{\mathrm{open}}^{(e,o)}$ in equation (5.8) can be regarded as effectively decoupled, if one is mostly interested in the effect on SSPP modes.

Thus, the main (and non-trivial) effect of the dielectric semi-infinite slab on SSPP in the open waveguide is the modification of the coupling parameter. For instance, the fundamental band is described by equation (4.1) with

$$\lambda=\frac{1}{2}\left(\lambda(\epsilon=1)+\frac{P^2(\epsilon)\kappa}{P^2\kappa(\epsilon)}\lambda(\epsilon)\right).\tag{5.9}$$

In particular, the SSPP plasma frequency, despite broken mirror symmetry, remains the same $\omega_p=\pi/h$, while the shift of the edge of the fundamental band is given by

$$\Delta\omega_e=\tfrac{1}{2}(\Delta\omega_e(\epsilon,1)+\Delta\omega_e(1,1))|_{h\to h/2}.\tag{5.10}$$

(c) Half-closed waveguide in contact with a thin dielectric layer

SSPP waveguides bounded by semi-infinite dielectric slabs demonstrate relatively simple spectrum owing to the absence of special characteristic frequencies characterizing states of the

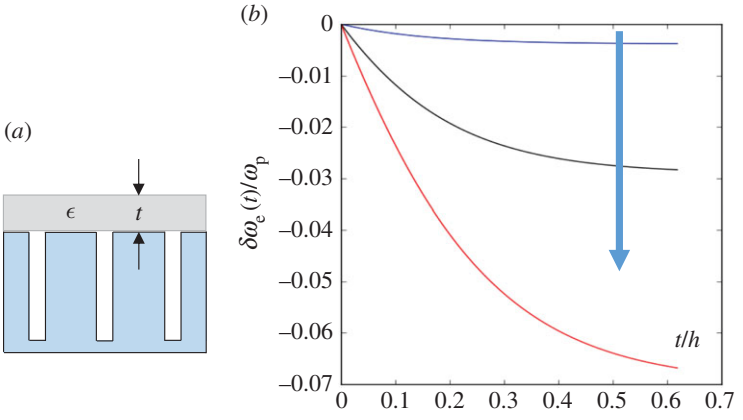

Figure 7. (*a*) The cross-section of an SSPP waveguide covered by a thin dielectric layer. (*b*) The variation of the edge of the fundamental SSPP band normalized by the effective plasma frequency with the thickness of the layer for different values of ϵ (the arrows shows the variation with increasing $\epsilon = 1.1, 1.7, 2.5$). (Online version in colour.)

field inside the dielectric. The situation is different when the structure is covered by a dielectric layer of finite thickness, t, (figure 7*a*). In this case, the relevant framework is provided by the approach based on coupled excitations as has been discussed in §3. We limit ourselves to consideration of a specific property of SSPP, sub-wavelength resolution. This property can be illustrated on the example of thin layers with $\epsilon \approx 1$, when waveguiding modes of the layer follow closely the vacuum light-line. As a result, in the SSPP regime, the states of the field inside the layer are attenuated and the effect of the layer on SSPP can be accounted for, with good approximation, by a modification of the coupling parameter. The SSPP dispersion equation is found from $\langle -1|\,\mathcal{T}\,|-x\rangle = 0$, with $\mathcal{T} = \mathcal{T}_{al}\mathcal{T}_l\mathcal{T}_{lg}\mathcal{T}_g$, where $\mathcal{T}_l = \mathrm{diag}(\exp(\mathrm{i}\hat{Q}(\epsilon)t), \exp(-\mathrm{i}\hat{Q}(\epsilon)t))$ is the transfer matrix through the layer and the interface transfer matrices are $\mathcal{T}_{al} = \mathcal{T}_i(\hat{T}_{\mathrm{U}}^{(1)}, \hat{T}_{\mathrm{U}}^{(2)})$ and $\mathcal{T}_{lg} = \mathcal{T}_i(\hat{T}_{\mathrm{D}}^{(1)}, \hat{T}_{\mathrm{D}}^{(2)})$, where $\hat{T}_{\mathrm{U}}^{(1,2)}$ are given by equation (2.23) with $\epsilon_{\mathrm{I}} = \epsilon$ and $\epsilon_{\mathrm{II}} = 1$, and $\hat{T}_{\mathrm{D}}^{(1,2)}$ are defined in equation (2.24) with $\epsilon_{\mathrm{I}} = 1$ and $\epsilon_{\mathrm{II}} = \epsilon$. Then, we obtain $D(\omega, \beta) = \cos(Ph) - \mathrm{i}\eta \sin(Ph)$, where

$$\eta = -\mathrm{i}(l = 0|\hat{T}_{\mathrm{D}}^{(2)}\hat{\lambda}_{\mathrm{L}}\frac{\hat{D}_{\mathrm{L}}^{(\mathrm{e})}}{\hat{D}_{\mathrm{L}}^{(\mathrm{o})}}\hat{T}_{\mathrm{D}}^{(1)}|l = 0), \tag{5.11}$$

with $\hat{\lambda}_{\mathrm{L}} = \mathrm{diag}(\lambda_{\mathrm{L},m})$ and $\hat{D}_{\mathrm{L}}^{(\mathrm{e,o})} = \mathrm{diag}(D_{\mathrm{L},m}^{(\mathrm{e,o})})$. Assuming that all higher Bloch modes with $|m| > 0$ are well attenuated, we obtain the same dispersion equation as for semi-infinite dielectric slab, equation (5.1), with modified $\lambda(\epsilon_{\mathrm{a}}) \to \lambda(\epsilon, t)$, where

$$\lambda(\epsilon, t) = \frac{a}{d}\left[\mathrm{sinc}^2\left(\frac{\beta a}{2}\right)\lambda_{\mathrm{L}}\frac{D_{\mathrm{L}}^{(\mathrm{e})}}{D_{\mathrm{L}}^{(\mathrm{o})}} + \frac{\kappa(\epsilon)d}{\pi}\left(\frac{3}{2} - \ln\left(\frac{2\pi a}{d}\right)\right)\right]. \tag{5.12}$$

The renormalization of the first term in the brackets distinguishes coupling with a thin layer from the case of semi-infinite slab. In view of equation (5.2), this renormalization describes the dependence of the edge of the fundamental band on the thickness of the layer. We extract this contribution into the position of the edge and define

$$\delta\omega_{\mathrm{e}}(t) = \omega_{\mathrm{p}}\frac{a}{d}\mathrm{sinc}^2\left(\frac{\beta a}{2}\right)\frac{2}{\pi\sqrt{(2h/d)^2 - 1}}\left(\frac{D_{\mathrm{L}}^{(\mathrm{e})}}{D_{\mathrm{L}}^{(\mathrm{o})}} - 1\right) \tag{5.13}$$

through the relations $\mathrm{d}\delta\omega_{\mathrm{e}}(t)/\mathrm{d}t = \mathrm{d}\omega_{\mathrm{e}}(t)/\mathrm{d}t$ and $\delta\omega_{\mathrm{e}}(t = 0) = 0$. The typical dependence of ω_{e} on the layer thickness is shown in figure 7*b*. The significant increase of the rate of shift of the edge

for small t with increasing ϵ can be seen directly from equation (5.13),

$$\frac{\mathrm{d}}{\mathrm{d}t}\delta\omega_{\mathrm{e}}(t)\bigg|_{t=0} = \frac{\omega_{\mathrm{p}}a}{dh}\mathrm{sinc}^2\left(\frac{\pi a}{2d}\right)\left(\epsilon - \frac{1}{\epsilon}\right). \tag{5.14}$$

It shows the sensitivity of the SSPP band edge to slight variations of ϵ close to 1. It should be noted, however, that the response of the band edge to the thickness variation reduces in structures with longer grooves due to the stronger attenuation of the field outside of the grooves.

6. Conclusion

We have presented a general framework for describing SSPP in periodic waveguides. The framework is based on extension of the transfer matrix approach in order to account for an infinite number of Bloch modes. While the formalism is developed for the example of SSPP waveguides with rectangular grooves perpendicular to the axis of the waveguide, various generalizations are relatively straightforward as long as the structure can be split in the transversal direction into regions communicating with each other through the field continuity boundary conditions on surfaces with a simple geometry. One of such generalizations would be to consider oblique grooves, which may be relevant for development of more efficient technological processes for growing SSPP structures with the operating frequency in the terahertz region. Another important generalization is to structures not bounded by conducting walls from the sides, which in many regards demonstrate features of the limit $w \to \infty$, owing to the fact that the distribution of the field inside the grooves is strongly restricted by their small width.

Taking into account an infinite set of Bloch modes leads to representation of a coupling parameter in the SSPP dispersion equation in terms of a series, which was usually truncated to the leading term yielding single Bloch mode approximation (SBMA). This approximation, while allowing for discussion of general properties, fails to reproduce accurately SSPP spectral properties near the edge of the band, where the SSPP effect is the most prominent. The transfer matrix approach for a full set of Bloch modes has allowed us to establish a relation of the coupling parameter with a Fourier series of a special function, which yielded a correction to the SBMA coupling parameter. The full coupling parameter is demonstrated to correctly account for the effect of higher Bloch modes in the SSPP regime. It is worth noting that the correction is stable with respect to structural modifications, thanks to the fact that higher Bloch modes are strongly attenuated and are affected only by an immediate vicinity of the groove opening. Not surprisingly, therefore, the correction appeared in the same form in various situations analysed in the paper.

We have applied the developed formalism to studying SSPP spectrum in different structures with the main attention paid to the position of the edge of the SSPP fundamental band, which plays an important role in the transport properties of SSPP. The main results are obtained for structures with heterogeneous distribution of the dielectric function. These structures, despite being important for adopting plasmon techniques to SSPP, did not enjoy theoretical attention because of difficulties in applying standard technical tools. We show that while the dielectric properties of the medium outside of the grooves do not modify the SSPP effective plasma frequency, the maximal Bloch wavenumber is downscaled leading to reduction of the SSPP region because of weaker attenuation in the dielectric.

Promising results are obtained for structures with grooves open at both ends. In these structures, the spectral properties of SSPP are determined by a coupling parameter 'averaged' over the openings of the grooves. This suggests the possibility to use these structures in set-ups, where spoof plasmons are excited at one side of the structure and interact with material applied at the opposite side: the geometry playing a very important role in plasmon applications.

Finally, we have studied the effect of a thin dielectric layer lying on top of the corrugated waveguide on the SSPP spectrum. We found that the position of the edge of the fundamental band is sensitive to variations of the thickness of the layer on sub-wavelength scale.

Data accessibility. The data represented by graphs was obtained from formulae provided in the main text.
Authors' contributions. M.E. conducted theoretical analysis and drafted the manuscript. S.R.J. carried out the numerical simulations and prepared some of the figures. P.M. contributed to development of the analytical model and revised the manuscript. All authors read and gave approval to the final version of the manuscript.
Competing interests. We have no competing interests.
Funding. The work was financially supported by the Air Force Office of Scientific Research (AFOSR) grant no. FA9550-12-1-0402 and by the National Science Foundation (NSF) grant no. 1116040.

References

1. Brillouin L. 1948 Wave guides for slow waves. *J. Appl. Phys.* **19**, 1023–1041. (doi:10.1063/1.1698006)
2. Chu EL, Hansen WW. 1947 The theory of disk–loaded wave guides. *J. Appl. Phys.* **18**, 996–1008. (doi:10.1063/1.1697586)
3. Pendry JB, Martin-Moreno L, Garcia-Vidal FJ. 2004 Mimicking surface plasmons with structured surfaces. *Science* **305**, 847–848. (doi:10.1126/science.1098999)
4. Hibbins AP, Evans BR, Roy Sambles J. 2005 Experimental verification of designer surface plasmons. *Science* **308**, 670–672. (doi:10.1126/science.1109043)
5. Garcia-Vidal FJ, Martin-Moreno L, Pendry JB. 2005 Surfaces with holes in them: new plasmonic metamaterials. *J. Opt. A: Pure Appl. Opt.* **7**, S97. (doi:10.1088/1464-4258/7/2/013)
6. Xiao B, Chen J, Kong S. 2016 Filters based on spoof surface plasmon polaritons composed of planar Mach–Zehnder interferometer. *J. Mod. Opt.* **63**, 1529–1532. (doi:10.1080/09500340.2016.1146805)
7. Zhang Q, Zhang HC, Wu H, Cui TJ. 2015 A hybrid circuit for spoof surface plasmons and spatial waveguide modes to reach controllable band-pass filters. *Sci. Rep.* **5**, 16531. (doi:10.1038/srep16531)
8. Zhang HC, Cui TJ, Zhang Q, Fan Y, Fu X. 2015 Breaking the challenge of signal integrity using time-domain spoof surface plasmon polaritons. *ACS Photon.* **2**, 1333–1340. (doi:10.1021/acsphotonics.5b00316)
9. Kong L-B, Huang C-P, Du C-H, Liu P-K, Yin X-G. 2015 Enhancing spoof surface-plasmons with gradient metasurfaces. *Sci. Rep.* **5**, 8772. (doi:10.1038/srep08772)
10. Gao X, Cui TJ. 2015 Spoof surface plasmon polaritons supported by ultrathin corrugated metal strip and their applications. *Nanotechnol. Rev.* **4**, 239–258. (doi:10.1515/ntrev-2014-0032)
11. Aghadjani M, Mazumder P. 2015 Terahertz switch based on waveguide-cavity-waveguide comprising cylindrical spoof surface plasmon polariton. *IEEE Trans. Electron Devices* **62**, 1312–1318. (doi:10.1109/TED.2015.2404783)
12. Quesada R, Martin-Cano D, Garcia-Vidal FJ, Bravo-Abad J. 2014 Deep-subwavelength negative-index waveguiding enabled by coupled conformal surface plasmons. *Opt. Lett.* **39**, 2990. (doi:10.1364/OL.39.002990)
13. Ma HF, Shen X, Cheng Q, Jiang WX, Cui TJ. 2014 Broadband and high-efficiency conversion from guided waves to spoof surface plasmon polaritons. *Laser Photon. Rev.* **8**, 146–151. (doi:10.1002/lpor.201300118)
14. Liu L, Li Z, Gu C, Ning P, Xu B, Niu Z, Zhao Y. 2014 Multi-channel composite spoof surface plasmon polaritons propagating along periodically corrugated metallic thin films. *J. Appl. Phys.* **116**, 013501. (doi:10.1063/1.4886222)
15. Shen X, Cui TJ, Martin-Cano D, Garcia-Vidal FJ. 2013 Conformal surface plasmons propagating on ultrathin and flexible films. *Proc. Natl Acad. Sci. USA* **110**, 40–45. (doi:10.1073/pnas.1210417110)
16. Fernandez-Dominguez AI, Moreno E, Martin-Moreno L, Garcia-Vidal FJ. 2009 Guiding terahertz waves along subwavelength channels. *Phys. Rev. B* **79**, 233104. (doi:10.1103/PhysRevB.79.233104)
17. Gan Q, Fu Z, Ding YJ, Bartoli FJ. 2008 Ultrawide-bandwidth slow-light system based on THz plasmonic graded metallic grating structures. *Phys. Rev. Lett.* **100**, 256803. (doi:10.1103/PhysRevLett.100.256803)
18. Kats MA, Woolf D, Blanchard R, Yu N, Capasso F. 2011 Spoof plasmon analogue of metal-insulator-metal waveguides. *Opt. Express* **19**, 14860–14870. (doi:10.1364/OE.19.014860)
19. Rusina A, Durach M, Stockman MI. 2010 Theory of spoof plasmons in real metals. *Appl. Phys. A* **100**, 375–378. (doi:10.1007/s00339-010-5866-y)

20. Ruan Z, Qiu M. 2007 Slow electromagnetic wave guided in subwavelength region along one-dimensional periodically structured metal surface. *Appl. Phys. Lett.* **90**, 201906. (doi:10.1063/1.2740174)
21. Garcia de Abajo FJ, Saenz JJ. 2005 Electromagnetic surface modes in structured perfect-conductor surfaces. *Phys. Rev. Lett.* **95**, 233901. (doi:10.1103/PhysRevLett.95.233901)
22. McVey BD, Basten MA, Booske JH, Joe J, Scharer JE. 1994 Analysis of rectangular waveguide-gratings for amplifier applications. *IEEE Trans. Microw. Theory Technol.* **42**, 995–1003. (doi:10.1109/22.293568)
23. Shen L, Chen X, Yang T-J. 2008 Terahertz surface plasmon polaritons on periodically corrugated metal surfaces. *Opt. Express* **16**, 3326–3333. (doi:10.1364/OE.16.003326)
24. Xu Z, Mazumder P. 2014 Terahertz beam steering with doped GaAs phase modulator and a design of spatial-resolved high-speed terahertz analog-to-digital converter. *IEEE Trans. Electron Devices* **61**, 2195–2202. (doi:10.1109/TED.2014.2318278)
25. Fernandez-Dominguez AI, Martin-Moreno L, Garcia-Vidal FJ, Andrews SR, Maier SA. 2008 Spoof surface plasmon polariton modes propagating along periodically corrugated wires. *IEEE J. Sel. Topics Quantum Electron.* **14**, 1515–1521. (doi:10.1109/JSTQE.2008.918107)
26. Maier SA, Andrews SR, Martin-Moreno L, Garcia-Vidal FJ. 2006 Terahertz surface plasmon-polariton propagation and focusing on periodically corrugated metal wires. *Phys. Rev. Lett.* **97**, 176805. (doi:10.1103/PhysRevLett.97.176805)
27. Aghadjani M, Erementchouk M, Mazumder P. 2016 Spoof surface plasmon polariton beam splitter. *IEEE Trans. THz Sci. Technol.* **6**, 832–839. (doi:10.1109/TTHZ.2016.2599289)
28. COMSOL Multiphysics 5.2. See http://www.comsol.com/.
29. Liu Y-Q, Kong L-B, Liu P-K. 2016 Long-range spoof surface plasmons on the doubly corrugated metal surfaces. *Opt. Commun.* **370**, 13–17. (doi:10.1016/j.optcom.2016.02.059)
30. Yao H, Zhong S. 2014 High-mode spoof SPP of periodic metal grooves for ultra-sensitive terahertz sensing. *Opt. Express* **22**, 25149. (doi:10.1364/OE.22.025149)
31. Wan X, Yin JY, Zhang HC, Cui TJ. 2014 Dynamic excitation of spoof surface plasmon polaritons. *Appl. Phys. Lett.* **105**, 083502. (doi:10.1063/1.4894219)